Electronic Supplementary Material (ESI) for ChemComm.

Supporting Information for

Quantitative determination of lithium depletion during rapid cycling in sulfide-based all-solid-state batteries

Sung Soo Shin,‡[a] Ji-Su Kim,‡[a] Sungjun Choi,[a] Ho-Il Ji,[a] Kyung Joong Yoon,[a] Jong-Ho Lee,[a] Kyung Yoon Chung,[b] and Hyoungchul Kim*[a]

[a]Center for Energy Materials Research, Korea Institute of Science and Technology, 5 Hwarang-ro 14-gil, Seongbuk-gu, Seoul 02792, Republic of Korea.
[b]Center for Energy Storage Research, Korea Institute of Science and Technology, 5 Hwarang-ro 14-gil, Seongbuk-gu, Seoul 02792, Republic of Korea.

‡These authors contributed equally to this work.

*Corresponding author (email: hyoungchul@kist.re.kr)

Experimental

Material Characterization. Using high-purity raw materials (Li_2S, P_2S_5, and LiCl, Aldrich) $Li_{5.5}PS_{4.5}Cl_{1.5}$ powder was synthesized as a solid electrolyte (SE) using a planetary ball mill (Pulverisette 6 Premium Line, Fritsch) at 700 rpm for 9 h. The detailed SE synthesis process can be found in a previous report.[1] The $LiNbO_3$ layer (0.25 wt.% based on NCM weight) was coated on the surface of commercial $LiNi_{0.6}Co_{0.2}Mn_{0.2}O_2$ (NCM, LNF) powder via a spray-drying method using ethanol-soluble anhydrous lithium nitrate ($LiNO_3$, Alfa Aesar) and niobium pentaethoxide [$Nb(OCH_2CH_3)_5$, Sigma-Aldrich]. The as-coated NCM powder was then annealed at 600 °C for 5 h in an electric furnace.

Transmission electron microscopy (TEM; Talos F200X, FEI; 200 kV) and X-ray diffraction (XRD; D8 Advance, Bruker) were used to confirm the morphology and crystalline structure of the NCM powder in the absence (NCM) and the presence of the $LiNbO_3$ coating (Nb-NCM) (Fig. S1). The microstructures of the tested cells were observed using scanning electron microscopy (SEM; Regulus 8230, Hitachi). The S 2*p* electronic structure was analyzed using X-ray photoelectron spectroscopy (XPS; PHI 5000 VerasProbe, Ulvac-PHI) with Al Kα (1486.6 eV) radiation. Spectral deconvolution was performed using Gaussian–Lorentzian functions in the MultiPac software (Ulvac-PHI). To prevent exposure to air, the samples were mounted in a glovebox and transferred to the analysis chamber using an Ar-filled transfer vessel.

Cell Fabrication. The composite cathode consisted of Nb-NCM or NCM as the cathode active material (CAM), $Li_{5.5}PS_{4.5}Cl_{1.5}$ as the SE, and vapor-grown carbon fiber (VGCF) as a conductive agent in a weight ratio of 60:36:4. The components were mixed with stainless-steel balls in a stainless-steel bowl using a vibration mixer mill (MM400, Retsch). All the cells were composed of a counter electrode of In metal, a SE of $Li_{5.5}PS_{4.5}Cl_{1.5}$, and the composite cathode. $Li_{5.5}PS_{4.5}Cl_{1.5}$ powder (0.05 g) was placed in a mold (10 mm diameter) and compressed at 192 MPa for 2 min. Then, the composite cathode (0.02 g) was spread on one side of the compressed SE and the sample was pressed at 317 MPa for 2 min. Subsequently, In metal foil (9 mm diameter and 100 μm thick) was placed on the other side of the compressed SE and the sample was pressed at 125 MPa for 3 s. Finally, three-layered pellet was assembled in a 2032-type coin cell for electrochemical measurements.

Cell Characterization. Electrochemical charge–discharge tests were conducted in the voltage range of 2.0–3.6 V (vs. In/InLi) at 25 °C using a battery testing system (4300K Desktop, Maccor). Cycling was performed at 1 C-rate (= 180 mA g^{-1}), and cells were charged and discharged in the constant current mode. Electrochemical impedance spectroscopy (EIS) analyses of the cells were carried out after a sufficient rest step until the potential reached equilibrium after charging to 3.6 V (*vs.* In/InLi) using a frequency response analyzer (1260, Solartron) and an electrochemical interface apparatus (1287, Solartron) at 25 °C. All EIS results were collected in the charged state in the frequency range of 5×10^{6}–1×10^{-2} Hz using a voltage perturbation with an amplitude of 50 mV. The EIS spectra were interpreted based on an equivalent circuit model (ECM) using the ZView software (Scribner Associates). The distribution of relaxation times (DRT) method was applied to reinterpret the EIS spectra using the intrinsic time constants. After fitting the raw spectra using the ZView software, the results, with the exception of the first semicircle in the high-frequency region (bulk resistance of the SE layer), were transformed to a regularization function [$\gamma(f)$] versus frequency by using FTIKREG program.[2] In the DRT results, the resistance value of each loss process was calculated based on areal proportions using Gaussian fitting. The detailed theoretical background for this analysis method can be found previous reports.[3,4]

Density Functional Theory (DFT) Calculations. To mimic the electrochemical deterioration of Li-argyrodite during delithiation, DFT calculation was performed using the Vienna *ab initio* simulation package (VASP) code.[5] The projected augmented wave method of Blochl and the generalized gradient approximation of Perdew, Burke, and Ernzerhof were introduced to describe the electron wave functions and the exchange correlation energy, respectively, in each calculation.[5–9] Using these computational settings, the $Li_{5.5}PS_{4.5}Cl_{1.5}$ unit cells were optimized with a 2 × 2 × 2 Monkhorst–Pack K-points mesh and a cutoff energy of 520 eV.[10] The lattice parameters and cell shape were allowed to relax during optimization. The valence electrons of the S and Cl ions in $Li_xPS_{4.5}Cl_{1.5}$ were analyzed using Bader charge analysis implemented in the VASP code.[11] The anion clusters in Fig. S5a were drawn using the VESTA program.[12]

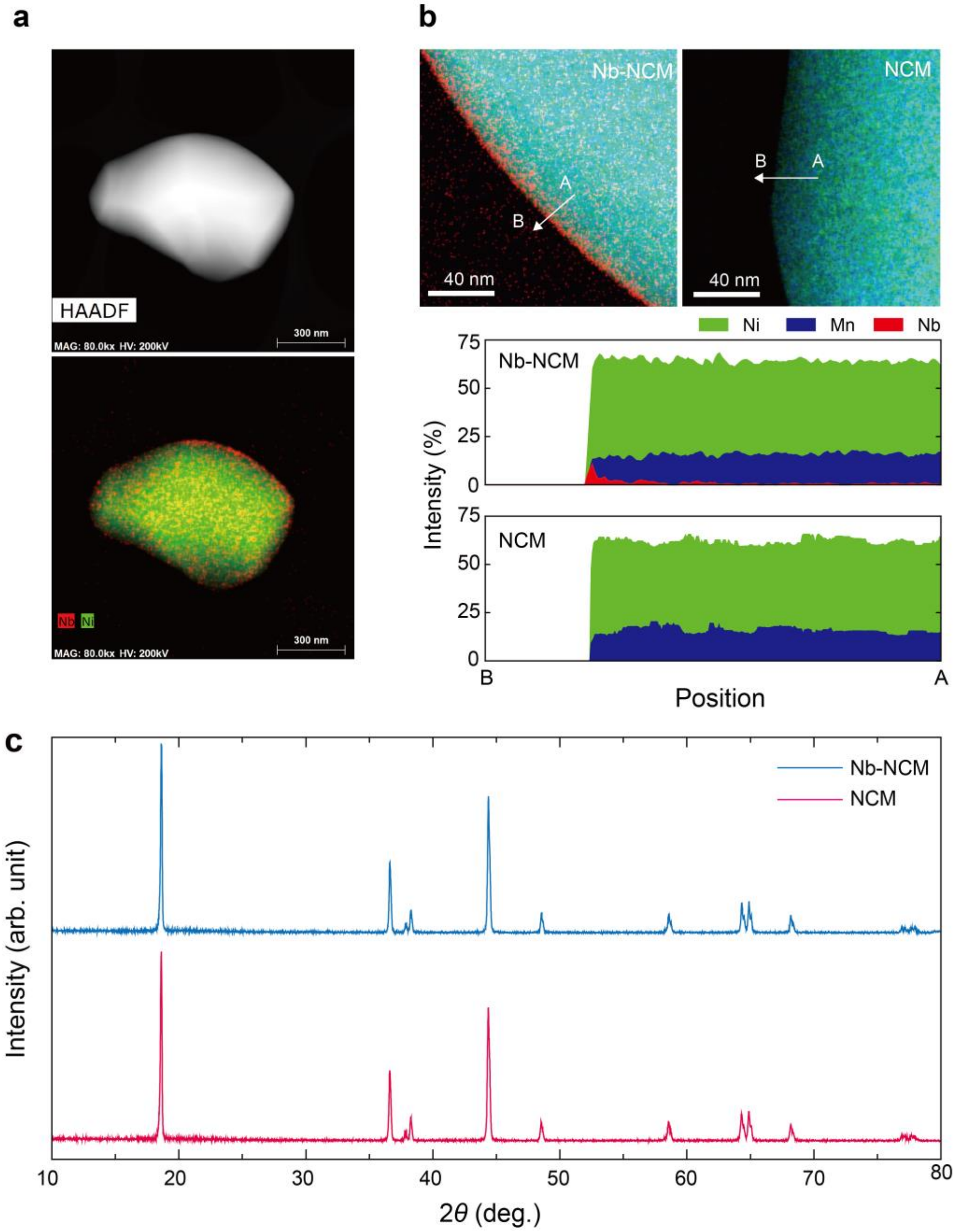

Fig. S1. (a) HAADF-STEM and energy dispersive X-ray spectroscopy (EDS) images of Nb-NCM powder. (b) Profiles of EDS line scan for Nb-NCM (upper) and NCM (lower). The white arrows indicate the scanning lines for EDS. The green, blue, and red colors indicate Ni, Mn, and Nb elements, respectively. (c) XRD patterns of Nb-NCM and NCM. There was no structural difference after coating, and any $LiNbO_3$ peaks were not detected owing to their small amounts (0.25 wt.%).

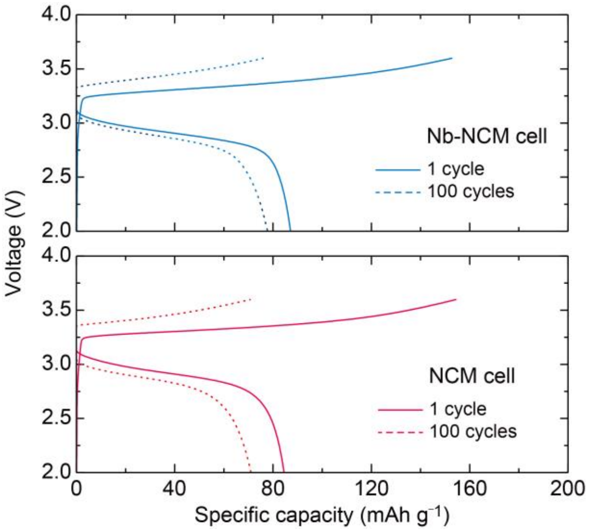

Fig. S2. Charge/discharge curves of Nb-NCM cell (upper) and NCM cell (lower) for selected cycles (1 and 100) at 1 C-rate, 25 °C. Relatively low coulombic efficiency, 57 %, was obtained due to the high 1 C-rate of the charging/discharging process. However, from the second cycle, high energy efficiency was confirmed by the maintenance of a coulombic efficiency greater than 99 %.

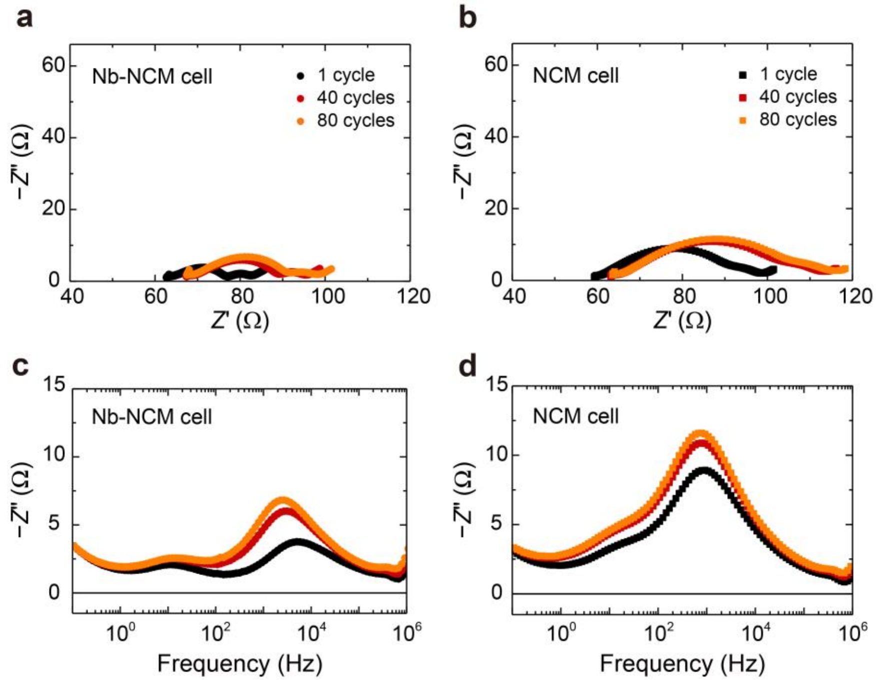

Fig. S3. Impedance spectra (Nyquist plots) of (a) Nb-NCM cell and (b) NCM cell measured after charging to 3.6 V (vs. In/InLi). Complementary impedance plots of (c) Nb-NCM cell and (d) NCM cell on –Z″ versus frequency.

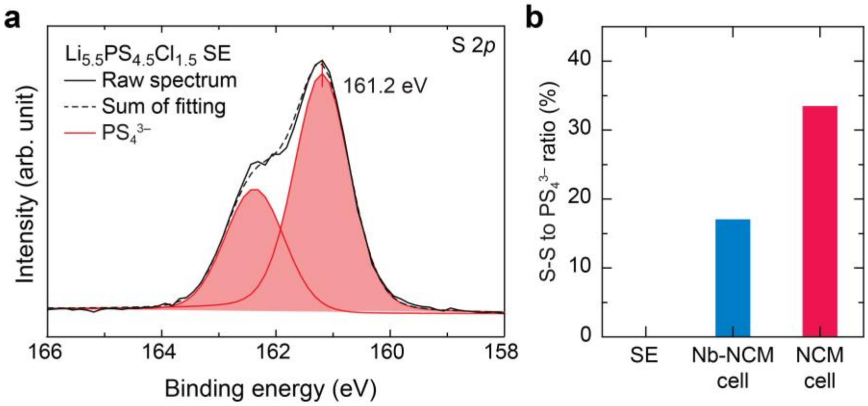

Fig. S4. (a) S 2*p* XPS spectra of $Li_{5.5}PS_{4.5}Cl_{1.5}$. The black line represents raw spectra while rest of lines (dotted black and red) show fitted lines. (b) Area ratio of S-S bonds to P-S bonds in PS_4^{3-} from the S 2*p* XPS spectra of $Li_{5.5}PS_{4.5}Cl_{1.5}$ SE and the composite cathode after 100 cycles for the Nb-NCM cell and NCM cell.

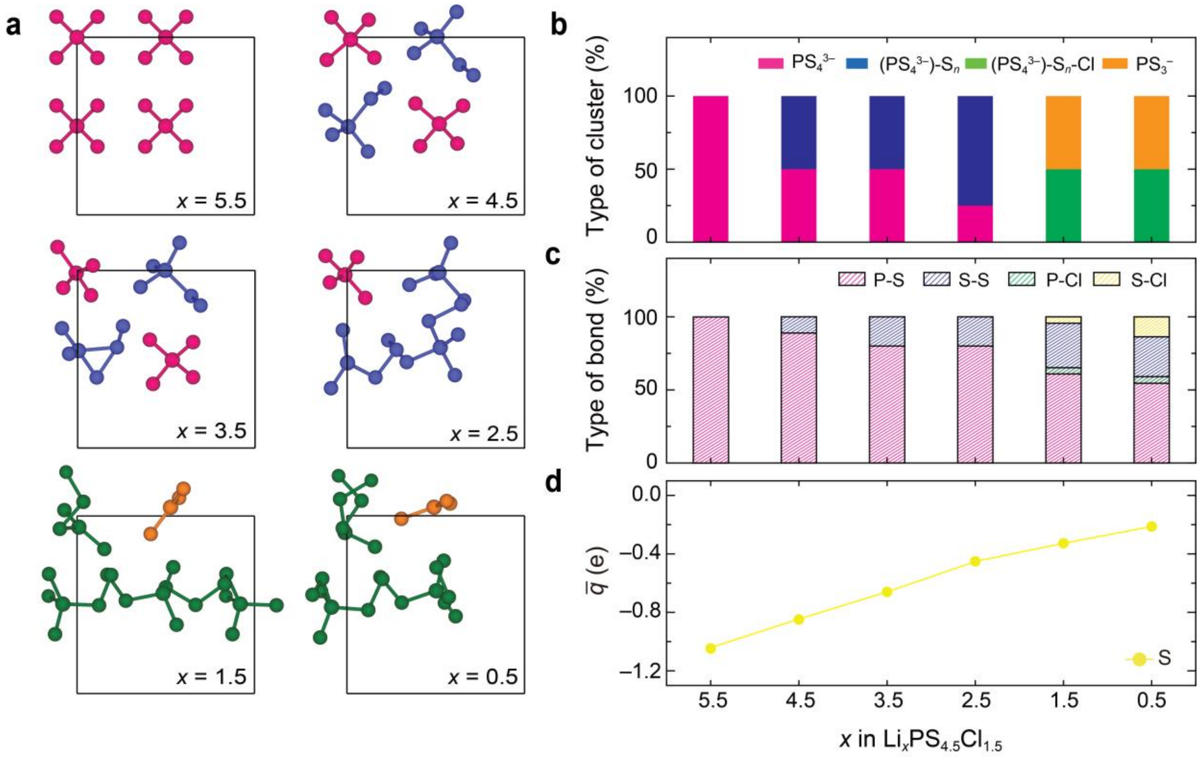

Fig. S5. (a) Identified anion clusters in delithiated $Li_xPS_{4.5}Cl_{1.5}$ ($0.5 \leq x \leq 5.5$) using DFT calculations. The cyan, blue, green, and orange colors indicate the PS_4^{3-}, (PS_4^{3-})-S_n, (PS_4^{3-})-S_n-Cl, and PS_3^{-} clusters, respectively. Type of (b) cluster and (c) bond in delithiated Li-argyrodite. The patterned cyan, blue, green, and yellow hatched squares indicate the P-S, S-S, P-Cl and S-Cl bonds, respectively. (d) Averaged valence charge ($\bar{q}$) of S ion in delithiated Li-agyrodite ($Li_xPS_{4.5}Cl_{1.5}$).

Table S1. Individual fitting component (R, CPE-T, CPE-P, C) values obtained from EIS curves by conventional fitting method of Nb-NCM cell and NCM cell at the 1, 40, and 80th cycle presented in Fig. 2.

Nb-NCM cell

	1st cycle	40th cycle	80th cycle
$R_{\text{SE-bulk}}$ [Ω]	62.0	67.0	66.0
$R_{\text{I-1}}$ [Ω]	4.7	5.0	6.3
CPE-$T_{\text{I-1}}$ [$Fs^{\alpha-1}$]	$1.00 \cdot 10^{-4}$	$3.00 \cdot 10^{-5}$	$8.00 \cdot 10^{-5}$
CPE-$P_{\text{I-1}}$ (α)	0.557	0.646	0.553
$C_{\text{I-1}}$ [F]	$2.22 \cdot 10^{-7}$	$2.38 \cdot 10^{-7}$	$1.73 \cdot 10^{-7}$
$R_{\text{I-2}}$ [Ω]	10.2	16.9	18.8
CPE-$T_{\text{I-2}}$ [$Fs^{\alpha-1}$]	$4.07 \cdot 10^{-5}$	$3.21 \cdot 10^{-5}$	$3.23 \cdot 10^{-5}$
CPE-$P_{\text{I-2}}$ (α)	0.752	0.762	0.764
$C_{\text{I-2}}$ [F]	$3.10 \cdot 10^{-6}$	$3.80 \cdot 10^{-6}$	$3.28 \cdot 10^{-6}$
$R_{\text{I-3}}$ [Ω]	4.4	5.1	5.1
CPE-$T_{\text{I-3}}$ [$Fs^{\alpha-1}$]	$6.21 \cdot 10^{-3}$	$5.51 \cdot 10^{-3}$	$5.72 \cdot 10^{-3}$
CPE-$P_{\text{I-3}}$ (α)	0.787	0.799	0.788
$C_{\text{I-3}}$ [F]	$2.34 \cdot 10^{-3}$	$2.25 \cdot 10^{-3}$	$2.21 \cdot 10^{-3}$

NCM cell

	1st cycle	40th cycle	80th cycle
$R_{\text{SE-bulk}}$ [Ω]	59.5	64.0	64.0
$R_{\text{I-1}}$ [Ω]	6.20	6.80	7.50
CPE-$T_{\text{I-1}}$ [$Fs^{\alpha-1}$]	$2.00 \cdot 10^{-4}$	$1.50 \cdot 10^{-4}$	$1.80 \cdot 10^{-4}$
CPE-$P_{\text{I-1}}$ (α)	0.554	0.579	0.551
$C_{\text{I-1}}$ [F]	$9.19 \cdot 10^{-7}$	$9.97 \cdot 10^{-7}$	$8.34 \cdot 10^{-7}$
$R_{\text{I-2}}$ [Ω]	25.4	30.9	32.9
CPE-$T_{\text{I-2}}$ [$Fs^{\alpha-1}$]	$7.23 \cdot 10^{-5}$	$6.47 \cdot 10^{-5}$	$6.39 \cdot 10^{-5}$
CPE-$P_{\text{I-2}}$ (α)	0.731	0.730	0.727
$C_{\text{I-2}}$ [F]	$7.10 \cdot 10^{-6}$	$6.51 \cdot 10^{-6}$	$6.32 \cdot 10^{-6}$
$R_{\text{I-3}}$ [Ω]	5.5	7.6	8.7
CPE-$T_{\text{I-3}}$ [$Fs^{\alpha-1}$]	$5.63 \cdot 10^{-3}$	$4.70 \cdot 10^{-3}$	$5.14 \cdot 10^{-3}$
CPE-$P_{\text{I-3}}$ (α)	0.770	0.741	0.716
$C_{\text{I-3}}$ [F]	$1.99 \cdot 10^{-3}$	$1.47 \cdot 10^{-3}$	$1.50 \cdot 10^{-3}$

Table S2. Values of interfacial resistances using DRT method in Nb-NCM cell and NCM cell at the 1, 40, and 80th cycle presented in Fig. 3.

Nb-NCM cell

	1st cycle	40th cycle	80th cycle
$R_{\text{SE-bulk}}$ [Ω]	62.0	67.0	66.0
$R_{\text{I-1}}$ [Ω]	3.6	4.9	5.9
$R_{\text{I-2}}$ [Ω]	10.4	15.8	17.8
$R_{\text{I-N}}$ [Ω]	0.9	1.2	1.3
$R_{\text{I-3}}$ [Ω]	4.4	5.1	5.2

NCM cell

	1st cycle	40th cycle	80th cycle
$R_{\text{SE-bulk}}$ [Ω]	59.5	64.0	64.0
$R_{\text{I-1}}$ [Ω]	4.7	6.1	6.5
$R_{\text{I-2}}$ [Ω]	23.4	27.7	29.6
$R_{\text{I-N}}$ [Ω]	3.5	3.7	4.4
$R_{\text{I-3}}$ [Ω]	5.4	7.8	8.6

References

1 W. D. Jung, J.-S. Kim, S. Choi, S. Kim, M. Jeon, H.-G. Jung, K. Y. Chung, J.-H. Lee, B.-K. Kim, J.-H. Lee and H. Kim, *Nano Lett.*, 2020, **20**, 2303–2309.

2 J. Weese, *Comput. Phys. Commun.*, 1992, **69**, 99–111.

3 H. Schichlein, A. C. Müller, M. Voigts, A. Krügel and E. Ivers-Tiffée, *J. Appl. Electrochem.*, 2002, **32**, 875–882.

4 S. M. Choi, H. An, K. J. Yoon, B.-K. Kim, H.-W. Lee, J.-W. Son, H. Kim, D. Shin, H.-I. Ji and J.-H. Lee, *Appl. Energy*, 2019, **233–234**, 29–36.

5 G. Kresse and J. Hafner, *Phys. Rev. B*, 1993, **47**, 558–561.

6 G. Kresse and J. Furthmüller, *Comput. Mater. Sci.*, 1996, **6**, 15–50.

7 P. E. Blöchl, *Phys. Rev. B*, 1994, **50**, 17953–17979.

8 G. Kresse and D. Joubert, *Phys. Rev. B*, 1999, **59**, 1758–1775.

9 J. P. Perdew, K. Burke and M. Ernzerhof, *Phys. Rev. Lett.*, 1996, **77**, 3865–3868.

10 H. J. Monkhorst and J. D. Pack, *Phys. Rev. B*, 1976, **13**, 5188–5192.

11 W. Tang, E. Sanville and G. Henkelman, *J. Phys. Condens. Matter*, 2009, **21**, 084204.

12 K. Momma and F. Izumi, *J. Appl. Crystallogr.*, 2008, **41**, 653–658.